



# Residual stresses in adhesively bonded wood determined by a bilayer flexion reporter system

Jonas Matthias Maas<sup>1</sup> · Phillipe Grönquist<sup>2</sup> · Jennifer Furrer<sup>1</sup> ·  
Vanessa Studer<sup>1</sup> · Anselmo Malveti<sup>1</sup> · Markus Rüggeberg<sup>1,3</sup> ·  
Falk K. Wittel<sup>1</sup>

Received: 27 September 2021 / Accepted: 26 July 2022 / Published online: 25 August 2022  
© The Author(s) 2022

## Abstract

The application of adhesives in modern timber engineering often introduces moisture into the wood, leading to permanent residual stresses after hardening. This paper proposes a novel approach to assess these residual stresses by using wooden bilayers as a reporter system. For thin bilayers, moisture-induced stresses lead to pronounced visible flexion that can be used to identify the stress-driving parameters of the adhesive's gelation process. These parameters depend solely on the wood/adhesive combination and are inversely determined by fitting a finite element method model on the experimentally obtained flexion state. In a subsequent step, the determined parameters are used to calculate the residual stresses in the adhesive bondline of cross-laminated timber plates, emphasizing this approach's scale independence and general applicability to larger scale structures. All combinations of European beech and Norway spruce with the adhesives Melamine–Urea–Formaldehyde (MUF), Phenol–Resorcinol–Formaldehyde (PRF), and Polyurethane (PUR) were investigated.

## Introduction

Adhesive bonding is the backbone of modern timber engineering, extending sizes, geometries, reliability, and many other key properties for design. This was enabled by impressive technical progress in adhesive formulations. For structural applications, adhesives based on polyaddition and -condensation reactions (Kollmann et al. 1975; Kumar and Pizzi 2019; Hunt et al. 2019) are common. The composition of adhesives and their respective chemistry of cross-linking often involves water release or uptake. Wood–water interactions in the adherent wood layers involve moisture transport (Siau 1984; Skaar 1988), hygro-expansion, and change of

---

✉ Jonas Matthias Maas  
jomaas@ethz.ch

Extended author information available on the last page of the article

mechanical properties (Kollmann and Cote 1968; Niemz and Sonderegger 2017). In an out-of-equilibrium system this inevitably results in fabrication-induced residual stresses (Kollmann et al. 1975; Gereke 2009; Hunt et al. 2019), that will superimpose with the regular stress field due to service loads. If stresses are uncertain, their effect on the load capacity is uncertain as well. Unfortunately, residual stresses are not comprised implicitly in standard adhesive bonding strength test cases, as summarized in Hänsel et al. (2021). According to DIN EN 301 (2017), DIN EN 302-1 (2013) and DIN EN 302-2 (2017) or ASTM D4501 (2014), shear strength has to be determined at small scale by shear tests, assuming that these strength values can be directly applied to the material development process of large-scale structural components. However, the residual stresses have relaxed (Niemz and Sonderegger 2017) as a consequence of the small-scale shear sample preparation due to cutting prior to the testing. Additionally, residual stresses are also size-dependent (Okkonen and River 1989; Hassani et al. 2016; Hänsel et al. 2021), resulting in an uncertainty of the remaining load bearing capacity of large-scale adhesively bonded wood components. Knowledge of the true superimposed stresses will potentially allow a less conservative construction approach. The fundamental problem of residual stresses lies in their experimental accessibility, rendering the direct experimental determination questionable. It is possible to determine internal stresses via stress/strain relief measurements when cutting cross sections (Archer 1987; Niemz and Sonderegger 2017). However, only selective stresses at specific points are measured, not allowing a universally valid prediction of the continuum, and extensive cutting of full-size samples is not always an option.

We demonstrate a combined experimental-numerical approach to universally estimate such fabrication induced residual stresses. This is possible by back-calculating the stress-driving properties from spatial flexion states of moisture-sensitive (Grönquist et al. 2018; Rindler et al. 2019) wood bilayers. Due to the limited kinematics of bilayer deflections, the respective samples are thin and slender to be sensitive to moisture changes (Wood et al. 2018; Rindler et al. 2019). The extracted parameters describing the bonding process are not size-dependent and can then be used to calculate residual stresses in larger scale structures, like cross-laminated timber (CLT) plates. In this study, all combinations of spruce and beech wood with Melamine-Urea-Formaldehyde (MUF), Phenol-Resorcinol-Formaldehyde (PRF), and one-component Polyurethane (1K-PUR) adhesives are evaluated. The experimental flexion and moisture content evolution after adhesive bonding of the bilayers and respective pressing is monitored at a constant climate. Two stress-driving parameters are identified controlling the flexion of the bilayers, called the gelation time  $t_{\text{gel}}$  and film coefficient  $\beta$ . In state-of-the-art simulations for hygro-mechanical wood-adhesive joints like in Bachtiar et al. (2019), the correct physical description of the wood-adhesive interface proved to be a challenge. These two parameters will allow a more detailed description of this interaction during the hardening process and its residual stresses. By fitting finite element method (FEM) simulations with hygro-elastic material behavior to the observed deformation of the bilayers, the parameters are inversely determined. To show the applicability of  $t_{\text{gel}}$  and  $\beta$  in larger scale structures, the most suitable parameter set is used in a subsequent step, where the residual stresses occurring in the adhesive layers of CLT plates are determined.

## Materials and methods

Wooden bilayers consist of an adhesively bonded active, driving layer and a passive, resisting layer. The flexion of the bilayer during moisture change, depicted in Fig. 1, is caused by a different fiber orientation in both layers. The different fiber orientations go along with different hygro-expansive properties and respective changes of the elastic parameters along their individual layer axes. During moisture change, the absolute flexion depends on the initial moisture content the wood had during hardening, resulting from the environmental climate the wood was equilibrated to and the water intake or outtake by the adhesive, as shown for example by Rindler et al. (2019). The underlying mechanisms are depicted in Fig. 2 with following stages:

- The bilayer is pressed. The adhesive is liquid and moisture diffuses into the active and passive layer. Their moisture content increases. No moisture is exchanged to the environment. The moisture gradient inside the wood layers and the constrained deformation leads to inner stresses.
- The adhesive is solid. The moisture content inside the wood increases further. The adhesive bonding leads to a superposition of moisture gradient stresses and compression in the active layer and tension in the passive layer, caused by the suppressed deformation.
- The bilayer is removed from press, releasing its deformation potential by curving. The bilayer curves due to the current moisture content, gelation state, and moisture diffusion of the adhesive to the wood. Because moisture is then exchanged with the environment, the overall moisture content decreases. With decreasing moisture, the curvature first decreases and eventually flips into increasing opposite curvature.

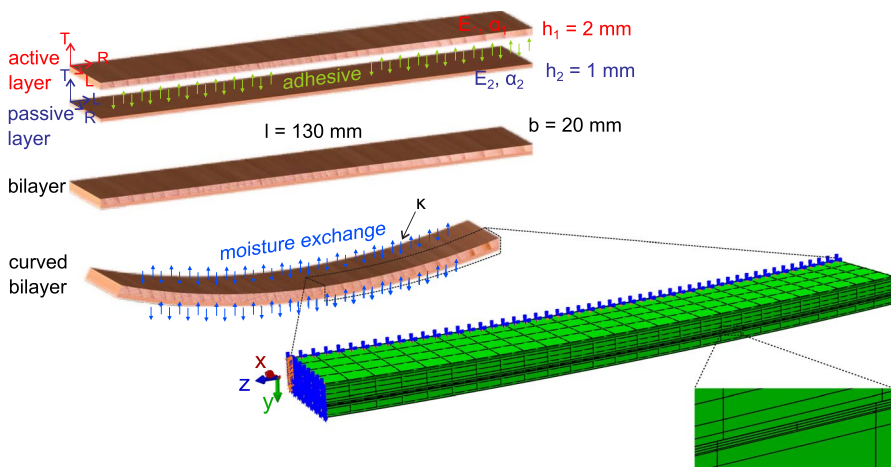


**Fig. 1** Active and passive layer in the wood bilayer including the fiber orientation and FE-mesh of the quarter model.  $E_1$  and  $E_2$  are the Young's moduli and  $\alpha_1$  and  $\alpha_2$  the swelling coefficients in radial (R) and longitudinal (L) direction, respectively.  $T$  is the tangential direction and  $\kappa$  the bilayer curvature

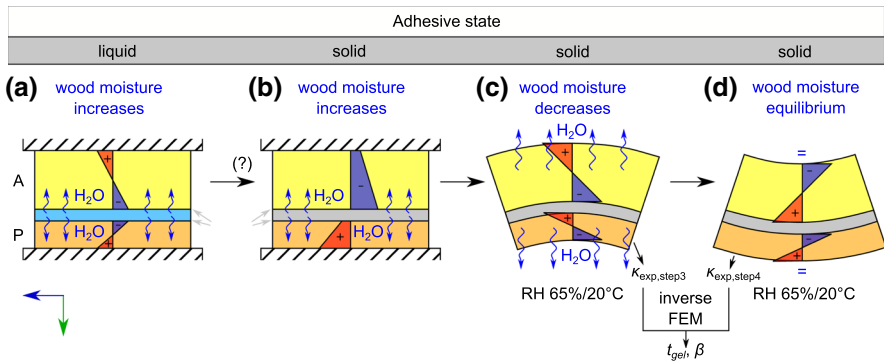


**Fig. 2** Concept of bilayer deformation for water intake (MUF and PRF). The experimental mean curvatures  $\kappa_{\text{exp,step3}}$  and  $\kappa_{\text{exp,step4}}$  are used in the inverse FEM calculation to obtain the unknown gelation time  $t_{\text{gel}}$  and film coefficient  $\beta$ . (+) and (–) indicate tensile and compressive stress in direction  $z$ .  $A$  and  $P$  indicate the active and passive layer. **a** Bilayer is pressed, adhesive is liquid. **b** Adhesive is solid. **c** Bilayer is removed from press and curves due to its moisture. **d** Bilayer moisture decreases until equilibrium with the environment

- (d) The bilayer moisture decreases until equilibrium with the environment is reached, resulting in an equilibrium curvature.

The corresponding parameters describing the bonding process and its respective water transport are obtained by conducting a set of experiments and inversely fitting a parameter-dependent FEM model onto the observed curvature. In section “[Experimental study](#)”, the setup of the experimental program is described, i.e., the preparation of the wood layers, the application of the adhesive and the measurement of curvature over time. This is followed by the numerical studies described in section “[Numerical approach](#)”, where in a first step a quarter of the bilayer according to Fig. 1 is simulated. The gelation time  $t_{\text{gel}}$  and film coefficient  $\beta$  are identified as the two stress-driving parameters. They are determined by simulating the bilayer experiments and using a surrogate model to fit the model onto the experimental curvatures. Followed by this in a second step, the determined parameters are used to investigate the development of adhesively introduced residual stresses in CLT plates.

## Experimental study

**Wood layer preparation:** Boards of Norway spruce (*Picea abies*) and European beech (*Fagus sylvatica*) wood, which had been air dried, were planed to 10 mm thickness and equilibrated in desorption to 65% relative humidity (RH) and 20 °C for two months. Boards with rift configuration, where the width of the boards is parallel to the radial (R) direction of the wood, were chosen, since the bilayer’s final layer thicknesses of 1 mm and 2 mm are in the range of typical growth ring widths. Rift configuration minimizes scatter and warping deformations of individual layers, and provides a rather uniform ring orientation throughout the whole sample.

**Bilayer configuration and preparation:** After equilibration, the boards were planed to their final thicknesses of 1 mm and 2 mm, respectively, and further cut down to strips of 130 mm length and 20 mm width. The length of the 2 mm thick strips corresponds to the anatomical R direction of the wood and the width to its longitudinal (L) direction. For the 1 mm strips, the fiber orientation is perpendicularly shifted and the length corresponds to the L direction, whereas the width corresponds to the R direction. Both layers were bonded in this  $[0^\circ, 90^\circ]$  lay-up, leading to the desired pure flexion behavior under moisture content change (Grönquist et al. 2018; Rüggeberg and Burgert 2015). The thicknesses of the wood layers were chosen to be as low as possible while simultaneously avoiding a penetration of the adhesive up to the outer wood surface. The thickness ratio of the active and passive layer was chosen as 2:1 to obtain a high sensitivity of bending (Rüggeberg and Burgert 2015; Li et al. 2016; Grönquist et al. 2018) while still having a thin active layer. Utilizing veneers was avoided, as veneers are altered in the wood–water interaction due to fabrication requirements, leaving them not suitable for such studies. The sample thicknesses were determined by using a micrometer screw, with an accuracy of 10 – 50  $\mu\text{m}$ .

**Adhesives for bilayer bonding:** Three types of commonly used wood adhesives and their bonding-related stress generation were tested: 1K-PUR, MUF, and PRF. The representative adhesives of the three different types are Kauramin 683 with hardener 688 for MUF, Aerodux 185 RL with hardener HP155 (Bolleter Composites) for PRF, and HB S309 (Henkel, Purbond) for 1K-PUR. Table 1 lists their relevant properties, like opening time, pressing time, and water content. Additionally, the number of samples per set is documented here. For each of the altogether six configurations, ten bilayers were initially manufactured. As not all the bilayers were considered qualitatively suitable after manufacturing and pressing for the beech/PRF configuration, only eight samples were used here for further evaluation. The applied amount of adhesive was determined by weight measurements immediately before the application of the adhesive and after taking the bilayers out from the press.

**Bilayer bonding:** For bonding, the bilayers were pressed in a hydraulic press with the manufacturer-recommended pressures and pressing times from Table 1. It was

**Table 1** Adhesive characteristics (manufacturer guidelines) and number of bilayer samples for MUF (BASF 2007), PRF (Bolleter Composites 2009) and PUR (Purbond 2011)

	MUF	PRF	PUR
Mixture adhesive/hardener	100/60	100/20	–
Amount [ $\text{g}/\text{m}^2$ ]	440	225	120–160
Application	DS	DS	SS
Open time [min]	50	8–10	30
Press time [min]	270	240	75
Pressure [MPa]	0.9	0.48–0.96	0.6–1
<i>Number of samples</i>			
Spruce	10	10	10
Beech	10	8	10

DS/SS = double/single-sided adhesive application

shown by Knorz et al. (2017) that the pressure itself does not have a considerable impact on the bonding behavior of cross-laminated wood. For pressing, guiding rails ensured the exact placement of the two layers and avoided relative movements during handling of the press (Electronic Supplementary Material ESM A, Fig. S1a). As pressing was done in a less well-controlled climate, the samples were sealed in thin plastic foil to minimize the water exchange with the environment. Reference samples without added adhesives were pressed in parallel to record any eventual change of weight due to the pressing environment. However, the weight changes proved to be insignificant. For PUR-bonded bilayers, no plastic foil was used because pretests did not show any influence of the environment. This was due to the short pressing time and the low moisture intake.

*Experimental schedule and climate conditions:* Weight and deflection images of the bilayers were recorded after gluing and pressing at regular time intervals up to 72 h after pressing for calculating the moisture content and curvature. First measurements were taken immediately after removing the bilayers from the press and detaching excess adhesive. The time intervals were increased from initially 20 min to finally 24 h. All curvature and weight measurements after pressing were conducted at 65% RH and 20 °C climate, identical to the climate conditions the samples were initially equilibrated to. RH and temperature were recorded every 2 min to capture eventual climate instabilities. However, the conditions remained constant for the entire period of this part of the study. Afterward, all samples were stored at 65% RH and 20 °C for 1 year before a second set of measurements was conducted. This set is serving as reference measurement for bilayer behavior in case of readily hardened adhesives. Again, weight and curvature were taken in these conditions before relocating the samples subsequently to 85%, 95%, back to 85% and 65% RH with the temperature kept at 20 °C. The samples were equilibrated for at least two weeks in the respective climate before recording weight and curvature.

*Measuring relevant wood and adhesive properties on matched reference samples:* As a plausibility check to literature data, the density and stiffness of each individual wood layer was determined before bonding. The Young's moduli in L and R direction were determined by 4-point bending on a Zwick Roell 10 with a 10 kN load cell in displacement-controlled mode up to a 4 mm displacement and a rate of 10 mm/min. The results are documented in Table S2, ESM C and proved to be sufficiently close to literature data. The wood moisture content and swelling coefficients in L and R direction were determined with reference samples manufactured simultaneously as twins to the bilayer samples (documented in Table S2). Wood moisture contents were determined by double-weight measurement at experimental condition and at oven-dry state after drying at 103 °C for 24 h. The swelling coefficients of the reference samples were determined by measuring the weight and dimension after equilibrating to 65%, 85%, and 95% RH at 20 °C for one week. The spatial dimensions were determined by taking images and evaluating them with ImageJ. The water loss of freshly mixed adhesives at 65% RH and 20 °C was determined by repeated weighing of pure adhesive samples over six months assuming an equilibrium moisture content at these conditions. According to Wimmer et al. (2013), the moisture contents at this climate after full curing are 2% (PUR), 6% (MUF), and 13% (PRF). Note that the moisture content loss in the samples differs from the

difference between initial and final water content because part of the water is bonded during the gelation process.

*Calculating moisture content and curvature:* For calculating the evolving moisture content of the bilayers over time, the weight of the samples was recorded with a precision of 0.1 mg. This weight was set into relation to the oven-dry mass of the bilayer, which is composed of the dry weight of the wood layers and the dry weight of the adhesive. The moisture content is defined as:

$$\omega = (m_{\omega} - m_{\text{dry}})/m_{\text{dry}}. \quad (1)$$

$m_{\omega}$  is the mass of the moist bilayer and  $m_{\text{dry}}$  its respective oven-dry mass. The dry weight of each wood layer and its moisture content at 65%/20°C climate was obtained from oven-dry measurements of the non-bonded reference samples. The reference samples were prepared under the same conditions. Then, subsequently, the dry weight of the adhesive was calculated from the weight of the bilayers after 1 year at 65%/20°C climate and the sorption isotherms in Wimmer et al. (2013). This was done via the following steps:

1. From the total weight of the bilayers after 1 year, the known weight of the wood layers (with known equilibrium moisture content) was subtracted, leaving the moist weight of the adhesive layer.
2. With the known equilibrium moisture contents of MUF, PRF, and PUR, the dry weights of the adhesive layers were determined.
3. Using the dry mass of wood and dry mass of adhesive, the average moisture content over the whole bilayer domain could be determined. This is done for every sample and measurement time by using its respective total mass.

Note that during the experiment in non-equilibrium conditions, it is not possible to further differentiate this moisture content into wood moisture and adhesive moisture.

The flexion of the bilayers was determined from the acquired images of the curved samples (ESM A, Fig.S1b). The images were converted to binary images and a second order polynomial function  $y = ax^2 + bx + c$  was fitted to the detected outer edges of the samples. Curvature  $\kappa$  was then determined within the interval  $0 \leq x \leq L$  with the sample length  $L$  to be:

$$\kappa = \frac{\ddot{y}(x)}{[1 + (\dot{y}(x))^2]^{3/2}}. \quad (2)$$

## Numerical approach

When back-calculating curvature via the analytic approach by Timoshenko (Timoshenko 1925) – originally formulated for thermostats, but also suitable for standard thin wood bilayers (Grönquist et al. 2018; Rüggeberg and Burgert 2015) – using the determined mass loss due to evaporation of the excess moisture from the adhesive, an up to three times larger curvature is predicted. Consequently,

not all excess moisture introduced by the adhesive is driving curvature. Since shear stress in the adhesive layers can only be transmitted in the solid state, the liquid-solid phase transition (gelation) of the adhesive plays an important role. This phenomenon cannot be considered in a simple analytical approach, calling for hygro-mechanical modelling with FEM. In the following work, this is implemented by a coupled thermal-mechanical analysis in Abaqus FEA.

Since the predictive quality with a simple nonlinear hygro-elastic material model was proven to be almost as good as with a full rheological model (Grönquist et al. 2018, 2019), the hygro-elastic model was chosen. As no large differences to the experimental data were observed, the moisture-dependent components of the compliance tensor of spruce (cubic dependence), beech (linear dependence), PRF (cubic dependence), and MUF (cubic dependence) are taken from Hassani et al. (2015, 2016) (Tables S3 and S4, ESM C), along with the moisture-dependent diffusion coefficients (Tables S5 and S6, ESM C). Moisture transport is modeled by Fick's second law for moisture diffusion. The swelling coefficients are considered as constant and taken from Hassani et al. (2015) (Table S7, ESM C). Because tangential data were required and the literature values are considered to be more accurate, the experimentally obtained swelling coefficients were used as a plausibility control. The model consists of three layers; the active and passive layer with respective anatomic orientation of the orthotropic material coordinate system, as well as an adhesive layer of 0.1 mm thickness. The mesh of all layers consists of quadratic coupled temperature-displacement hexahedral elements with reduced integration, as shown in the quarter model in Fig. 1. In gravimetric measurements of the water loss of the MUF and PRF bilayer samples in 65%/20 °C climate, a mass loss ( $\pm$  standard deviation) of  $0.4416 \pm 0.0134$  g/g<sub>MUF</sub> and  $0.2947 \pm 0.0499$  g/g<sub>PRF</sub> for beech and  $0.4585 \pm 0.0175$  g/g<sub>MUF</sub> and  $0.3488 \pm 0.0071$  g/g<sub>PRF</sub> for spruce was determined over a total time period of 1 year. With this, the total mass of diffusive water induced by the adhesive is determined, assuming that the active and passive layer were in moisture equilibrium with respect to the ambient climate. The initial water content of the adhesive  $\omega_{\text{adh,init}}$  is calculated as

$$\omega_{\text{adh,init}} = \omega_{\text{adh,equb}} + \frac{m_{\text{loss}}}{\rho_{\text{adh,fem}} \cdot V_{\text{adh,fem}}}, \quad (3)$$

where  $\omega_{\text{adh,equb}}$  is the equilibrium moisture content at 65%/20 °C climate,  $m_{\text{loss}}$  is the total mass loss after equilibrating in this climate,  $\rho_{\text{adh,fem}}$  is the dry density of the adhesive in the FEM model and  $V_{\text{adh,fem}}$  is the corresponding volume. For verification, the equilibrium moisture content developing over the whole bilayer without moisture transport to the environment was simulated. It matches the values expected from the experimental mass balances. More information on this verification can be found in ESM B. The entire gluing procedure is simulated as a four step procedure to cope with changing boundary conditions, namely:

Step 1: Constraining bending inside the press, applied as a symmetry boundary condition in *y*-direction (see Fig. 1) on the upper and lower outer face of the bilayer. The adhesive is in liquid state with its initial moisture content. The con-



tact between the wood strips and the adhesive is frictionless. Moisture transport from the adhesive layer into contacting wood layers is limited by a film coefficient  $\beta$  and no transport across system boundaries is occurring. Note that the step is limited by the gelation time  $t_{\text{gel}}$  of the adhesive that is more than its open time and will be identified inversely in the following.

- Step 2: After gelation, the adhesive is kinematically tied to the wood layers, while the compression and moisture boundary conditions remain like in step 1, until the full press time of the adhesive is reached.
- Step 3: The compressive stress is removed and the system elastically equilibrates without exchange of moisture with the environment.
- Step 4: Moisture transport across the outer system boundaries is added by defining the moisture content at the outer surfaces to their equilibrium moisture content at 65%/20 °C climate (taken from Table S2 for the wood and Wimmer et al. (2013) for the adhesive). In a transient simulation, the moisture transport across the boundary is simulated until reaching moisture equilibrium for the whole bilayer domain.

The approach is based on the idealizing assumptions that gelation is an instantaneous process and that the moisture release of the adhesive, originating from solvent and the water condensate from the polycondensation reaction, is controlled by a constant film coefficient and evolving moisture gradients. The film coefficient  $\beta$  describes the speed of moisture transport normal to the wood adhesive interface. It controls how fast moisture is exchanged between the adhesive and the wood. The gelation time  $t_{\text{gel}}$  is the time after sample preparation when the phase change of the adhesive from liquid to solid state is assumed. In liquid state, the adhesive is assumed to act as lubricant and no tangential forces can be transferred from the adhesive to the wooden layers. In solid state, the tangential bonding changes to a rough formulation. Therefore, while  $\beta$  describes how fast the active and passive layer are swelling,  $t_{\text{gel}}$  defines the point in time when the residual swelling strains get “frozen” with respect to each other. This is the result of the tight interface connection provided by the hardening of the adhesive.

The assumption of a discrete time of hardening  $t_{\text{gel}}$  is a strong simplification. As suggested in Zhu and Zhou (2010), the residual stresses in adhesively bonded wood strongly depend on the assumed friction coefficient of the adhesive bondline. Naturally, the friction coefficient evolves over time and is also pressure-dependent. In addition, the adhesive behaves like a thixotropic Bingham fluid. By defining the discrete time  $t_{\text{gel}}$ , where full-slip transitions to no-slip, such complex behavior gets smeared to one simple mechanism. Hereby, it becomes feasible for a simulation model by using only one parameter.

Both parameters  $\beta$  and  $t_{\text{gel}}$  have to be determined inversely by an optimization procedure that minimizes the offset between predicted and measured curvature at the end of steps 3 and 4. Experimental data for step 4 is collected from the samples equilibrated to 65%/20 °C climate for 1 year. For solving the minimization problem, the MATLAB® surrogate model toolbox MATSuMoTo (Mueller 2014) is used with the parameters depicted in Table 2. The offset of this minimization problem is characterized as the relative 2-norm of the difference between the vector containing

**Table 2** Input parameters of MATSuMoTo (Mueller 2014) to fit the film coefficient  $\beta$  and gelation time  $t_{\text{gel}}$  of the FEM model to the experimentally observed data

Setting	Property
Domain bounds hardening time (MUF/PRF) [h]	[0.1, 4.4]/[0.1, 3.9]
Domain bounds film coefficient (MUF/PRF) [ $\text{mm}^2/\text{h} \cdot 10^{-2}$ ]	[0.001, 0.1]/[0.001, 0.1]
Surrogate model	Reduced cubic regression polynomial
Sampling technique	Randomized sampling with local perturbation around the best solution, with additional points uniformly distributed along the input domain
Initial experimental design	Latin hypercube sampling

the predicted mean curvatures  $\kappa_{\text{fem}}$  after step 3 and 4 and the corresponding experimental mean curvatures  $\kappa_{\text{exp}}$  as  $\|\kappa_{\text{fem}} - \kappa_{\text{exp}}\|_2 / \|\kappa_{\text{exp}}\|_2$ . The simulations allow the determination of the residual stress distributions in the bilayer and adhesive bond-line in particular.

The fitted film coefficients  $\beta$  and gelation times  $t_{\text{gel}}$  are used in a subsequent simulation to calculate the residual stresses induced by adhesive moisture during the gluing process of a CLT plate. For comparability, the same plate geometry as in Hassani et al. (2016) is used. The plate's surface area is  $100 \text{ mm} \times 100 \text{ mm}$  with a thickness parameter  $d = 30 \text{ mm}$ , as shown in Fig. 3. An increased thickness will result in restrained bending and therefore residual stresses in the cross section while gluing. In the simulation, an eighth of the plate is simulated by applying symmetry boundary conditions along the plate's three central symmetry planes. Please note that in comparison to the bilayer simulation the symmetry plane along the thickness of the

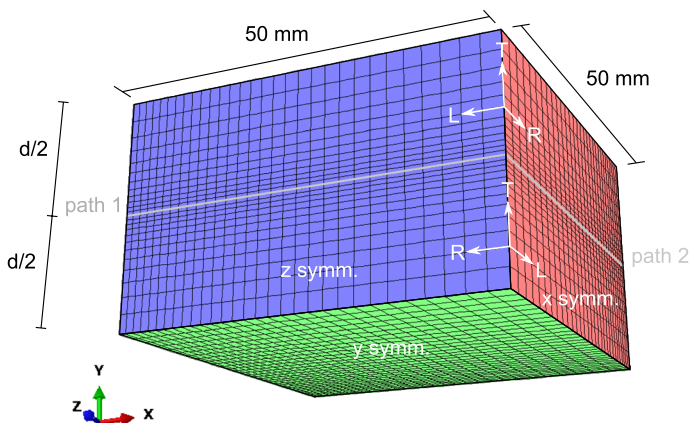


**Fig. 3** Geometry, anatomical direction (in Cartesian coordinates), and mesh of the cross-laminated timber simulations with the thickness parameter  $d = 30 \text{ mm}$ . The three visible faces are symmetry planes normal to  $x$ ,  $y$ , and  $z$  direction, respectively. The faces on the back side are no symmetry planes. Path 1 and 2 are paths along the adhesive interface

board (bottom plane in Fig. 3) got introduced. This changed the model from a simulation of two layers of wood with one adhesive layer to a simulation of three layers of wood with two adhesive layers. Besides, all other parameters of the model are the same as in the bilayer simulations, including the steps of the gluing procedure.

## Results and discussion

The experimental outcome, being the input for the subsequent parameter identification, can be found in section “[Bilayer flexion observations](#)”. The curvatures and mass loss over time are documented and used to describe the relation between curvature and average bilayer moisture content. Following in section “[Identification of control parameters for bilayer flexion](#)”, the inversely determined parameters  $t_{\text{gel}}$  and  $\beta$  based on this data are documented. These scale-independent parameters are used in the subsequent CLT plate simulations, where the corresponding peeling and shear stresses in the adhesive layer are described (section “[Estimation of residual stress in CLT](#)”). Furthermore, to quantify the influence of the layer thickness  $d$  on the model, the influence of the plate’s thickness on the total strain energy is investigated.

### Bilayer flexion observations

*Curvature at release from press:* For the bilayers bonded with the water-based adhesives MUF and PRF, negative curvatures of down to  $-0.58 \text{ m}^{-1}$  were observed immediately after release from the press. In contrast, positive curvatures of up to  $0.8 \text{ m}^{-1}$  were measured for PUR bonded bilayers (Fig. 4), being consistent to observations in Knorz et al. (2016). The initial negative curvatures, which indicate swelling of the active layer, can be explained by the up-take of water into the wood layers out from the water-based polycondensates MUF and PRF. Contrary, the positive curvatures of the PUR-bonded bilayers indicate a shrinking of the active layer and thus a withdrawal of water from the wood layers. The cross-linking and hardening of PUR is based on water uptake, but the amount of water needed for this reaction is supposed to be too low to cause such a magnitude of curvature. This assumption is supported by the very small decrease in curvature over time, indicating only a minor re-swelling of the active layer throughout the observed experimental time frame for the PUR-bonded bilayers. Consequently, the change of moisture content at the adjacent wooden layers during hardening was small as well. The low change of curvatures may indicate that PUR develops lower residual stresses due to pure water uptake than MUF or PRF. However, it does not necessarily imply that PUR will be the more advantageous adhesive, since the bonding strength depends mainly on the wood-adhesive interaction and curvatures (following from stresses from other sources) still developed in the PUR samples. Tests in Konnerth et al. (2016) show furthermore lower glue joint strengths for PUR than for MUF or PRF.

*Mass loss, moisture content change and curvature over time:* After transferring the bilayers from the press back into the reference climate, immediate mass losses were observed. After three days, these losses increased to up to  $-0.35 \text{ g}$  for

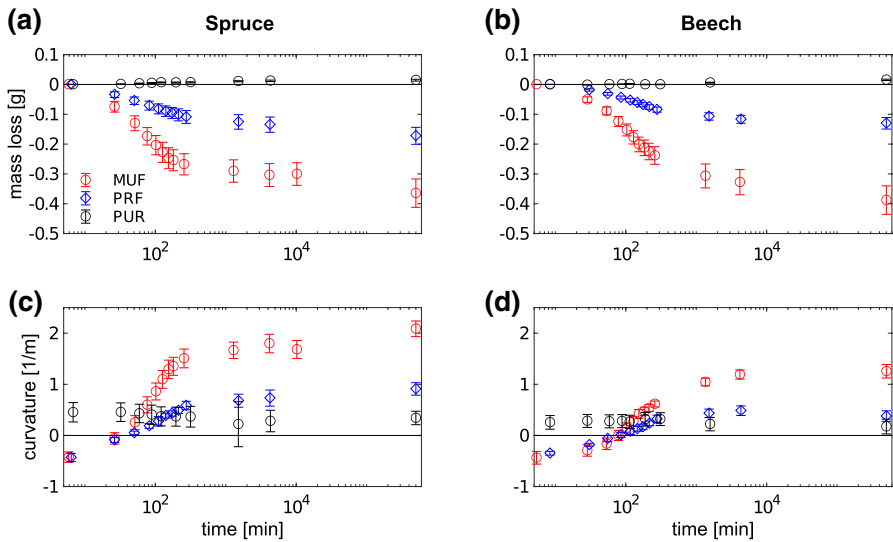


**Fig. 4** Evolution of mass loss and curvature for all configurations. **a** Mass loss spruce; **b** mass loss beech; **c** curvature spruce; **d** curvature beech

the MUF and PRF samples. This is caused by the re-equilibration of the bilayers to the reference climate (see Fig. 4), since an increased moisture was induced into the system by the adhesive. The observed mass loss of MUF samples was more than twice as high as for PRF bilayers. This can be explained by the amount of MUF being used for bonding, which was, following the suggestions of the suppliers in Table 1, approximately twice as high as PRF. Subsequently, MUF introduced significantly more water into the bilayer. Corresponding to the mass loss and reduction in water content, curvature evolved over time during re-equilibration, switching from negative to positive curvature (Fig. 4). In accordance with the weight measurements, the curvatures of the MUF bonded bilayers were also nearly twice as high as for PRF. The change of curvature for beech was less than that for spruce, as the same amount of weight loss, i.e., water loss, leads to a lower shift in moisture content due to a higher wood density. A very slight increase in mass and change of curvature was observed for the PUR bilayers, which shows that the bilayers were close to equilibrium conditions during the entire measurement period. The PUR samples may serve as control measurements for climatic conditions over time. The moisture equilibration is driven by diffusion and was almost completed for the thin wood layers of the MUF and PRF bonded bilayers within 72 hours after release from press (Fig. 4).

Curvature and weight measurements after 1 year of storage under identical climatic conditions (65%/20 °C) revealed hardly any shift in weight for the PUR-bilayers, legitimating the samples as reference samples for equilibrated moisture contents of wood and adhesives. In contrast, the MUF and PRF bonded bilayers revealed a further mass loss, i.e., water loss. This shows that an extended time frame larger than 72 h is required for full equilibration. Therefore, the measurements after 1 year

are taken as reference measurements for calculating the moisture content of the bilayers (Fig. 5).

In a subsequent step after 1 year, the bilayers were successively equilibrated to 85%, 95%, 85%, and 65% RH. Their respective moisture contents and curvatures were analyzed, with the resulting relationship being shown in Fig. 5. All configurations of the first set of measurements in the non-equilibrated state are compared to the second set in equilibrated state, 1 year later. Naturally, the range of moisture contents is different for the respective bilayer configurations. Differences in the behavior between the first and the second set become readily visible when comparing the specific curvature changes, visible as slope of the individual data series.

### Identification of control parameters for bilayer flexion

To determine the stress-driving gelation parameters, the experimental curvatures and moisture contents directly after pressing and after 1 year are used. The data are limited to MUF and PRF, since the curvature changes of PUR are too small to lead to trustworthy results. The fitted gelation times  $t_{\text{gel}}$  and film coefficients  $\beta$  of the bilayer models are documented in Table 3. It can be observed that for both beech and spruce,  $t_{\text{gel}}$  for PRF is smaller than for MUF. This matches the manufacturer's data in Table 1, where PRF has a lower curing time than MUF. In consistency to Rindler et al. (2019), the curvature of MUF bilayers after step 4 is higher than for

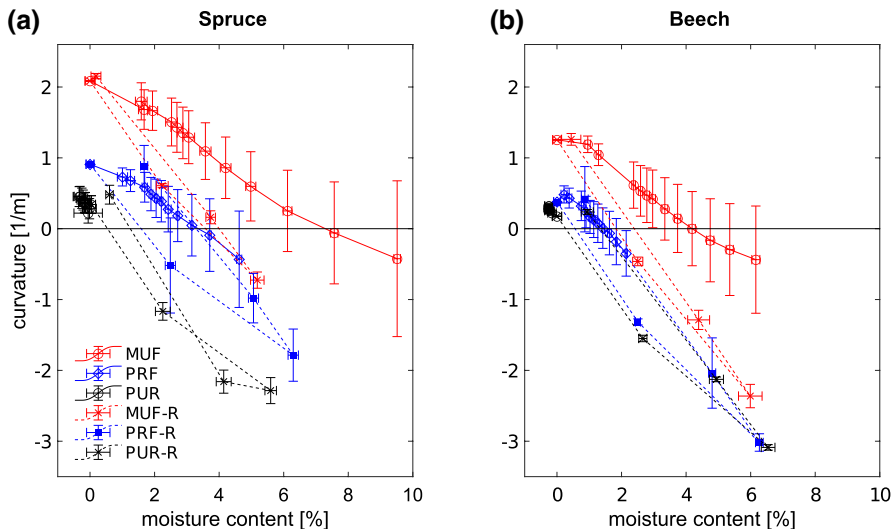


**Fig. 5** Curvature versus homogenized moisture content from mass balances (Eq. 1) for all configurations. Hereby, data in moisture content are shifted for better comparability: 0% moisture content is assigned to the measured equilibrated moisture content at 65%/20 °C climate. The suffix -R indicates data from the reference measurements of the samples after 1 year. Whereas in the original measurements moisture was still diffusing inside the bilayers, the samples at the reference measurements were subsequently equilibrated to 85%/95%/85%/65% RH at 20 °C. **a** Spruce; **b** beech

**Table 3** Inversely determined film coefficient  $\beta$  and gelation time  $t_{\text{gel}}$  and the corresponding curvatures  $\kappa$  and maximal stresses of the bilayer

	Beech		Spruce	
	MUF	PRF	MUF	PRF
Gelation time $t_{\text{gel}}$ [h]	0.82	0.26	1.52	0.95
Film coeff. $\beta$ [ $\text{mm}^2/\text{h} \cdot 10^{-2}$ ]	$1.23 \cdot 10^{-2}$	$3.25 \cdot 10^{-2}$	$8.43 \cdot 10^{-3}$	$1.19 \cdot 10^{-2}$
Experimental curvature after step 3 $\kappa_{\text{exp},3}$ [1/m]	-0.437	-0.359	-0.424	-0.431
FEM curvature after step 3 $\kappa_{\text{fem},3}$ [1/m]	-0.442	-0.358	-0.393	-0.449
Experimental curvature after step 4 $\kappa_{\text{exp},4}$ [1/m]	1.288	0.378	2.086	0.910
FEM curvature after step 4 $\kappa_{\text{fem},4}$ [1/m]	1.271	0.381	2.083	0.910
Relative 2-norm [-]	0.013	0.006	0.015	0.017
Max. shear stress [MPa]	6.129	2.400	4.757	1.205
Max. peeling stress [MPa]	5.387	1.667	6.357	1.184

The relative 2-norm is the 2-norm of the relative difference between experimental and FEM curvature

PRF bilayers, as MUF induces more water into the system, leading to larger hygro-expansion during hardening.

While comparing the different wood types, it is noticeable that  $t_{\text{gel}}$  for beech is remarkably lower than for spruce and simultaneously  $\beta$  is higher. The higher value for the film coefficient, representing a higher moisture conductance, can be explained by looking into the wood's cell structure. As it can be observed in SEM and  $\mu$ -CT scans in Hass et al. (2012), the moisture transport in softwood is dominated by cell wall transport, whereas for hardwood it is dominated by transport through the vessel network. The deep interconnection of the vessels and their generally more efficient water transmission lead to a higher moisture conductance. Simultaneously, it raises the risk that water and low molecular fractions might be quickly transported away from the adhesive, reducing the gelation time further. For spruce, the exclusive transport through the cell walls results in a low water transmission (Siau 1984; Hunt et al. 2019). Additionally, the finer anatomical structure leads to a low contact area of the adhesive to the wood (Konnerth et al. 2008; Gindl et al. 2004). This is unlike beech, where the adhesive strongly penetrates the vessel network before its viscosity increases, leading to a large contact area to the vessel's walls (Mendoza et al. 2012; Hass et al. 2012). Larger contact area and faster water transmission are considered to be the main reasons for beech's lower gelation time  $t_{\text{gel}}$  and higher film coefficient  $\beta$ .

Describing the hardening behavior of the adhesive by a discrete gelation time  $t_{\text{gel}}$  is a simplification that smears the wood-adhesive interaction during hardening. Alternatively to this approach, the friction coefficient in the adhesive bondline could be formulated as a function of time. However, as more unknown parameters and an arbitrary function shape would be involved, the scientific basis of the parameter fit by the surrogate model would rather be of mathematical than physical nature. Therefore, this approach was not favored. A global minimum of the minimization formula

of the surrogate model over its whole domain allowed a unique determination of the gelation time and film coefficient.

Note that the hereby applied bilayer model has limitations for long-term studies. The model does neither contain viscoelasticity nor mechanosorption or plasticity. Therefore, no relaxation in the samples is considered. Furthermore, the expansion coefficients are considered to be constant over the whole moisture domain up to fiber saturation. The water intake or outtake from the adhesive implies that wooden bilayers will never be plane if the initial wood moisture content equals the reference moisture, what proved to be a challenge in the production of weather-dependent self-actuating building parts in Wood et al. (2018). Calculating the required initial moisture contents for creating plane bilayers becomes possible by the hereby introduced parameters.

### Estimation of residual stress in CLT

A practical application of the bilayer's gelation parameters is the determination of moisture-induced residual stresses in CLT plates. This is possible because of the scale independence of  $t_{\text{gel}}$  and  $\beta$ . It follows the core ideas that hardening is controlled by the adhesive and moisture transport is controlled by the wooden material. Figure 6 and Table 4 document the peeling and shear stresses inside the adhesive layer, resulting from the FEM simulations, along the paths 1 and 2 (Fig. 3).

In general, it can be observed that the peeling stress in step 3 tends to be the dominant stress component. This is caused by a moisture gradient still being present in the wooden layers after pressing, which aspires the outer layer to bend such that it would open a gap at the outer edges of the adhesive layer. Since beech develops a stronger distributed moisture change and faster water uptake, the peeling stress is more pronounced here. In step 4, the shear stresses are large, because of the swelling differences that were present between the active and the passive layer in L and R direction when the adhesive hardened. When the water content of wood changes back during equilibration and back-transformation to its initial shape, the different swelling potential between the wooden layers gets activated. At the same time, with moisture gradients not being present in the wood anymore, the bending potential of the wood gets reduced, decreasing the peeling stress. When comparing the shear stresses between step 3 and step 4, the absolute shear in step 3 is generally smaller and the respective shear in step 4 and signs are inverted.

Regarding the influence of the material, it can be observed that MUF leads to stronger delamination stresses than PRF. This is due to the much higher moisture content introduced by MUF. Simultaneously, stresses for beech are higher than for spruce. Reasons are the higher stiffness, slightly higher swelling and fast transport that leads to a distribution of the moisture gradient over a larger cross-sectional area and a higher water uptake in general. This subsequently increases the residual stresses at step 4 as well. It is remarkable that beech already develops strong shear stresses at step 3. This can be explained by the low gelation time  $t_{\text{gel}}$  of beech, as seen in Table 3. The amount of shear depends on the difference of moisture content

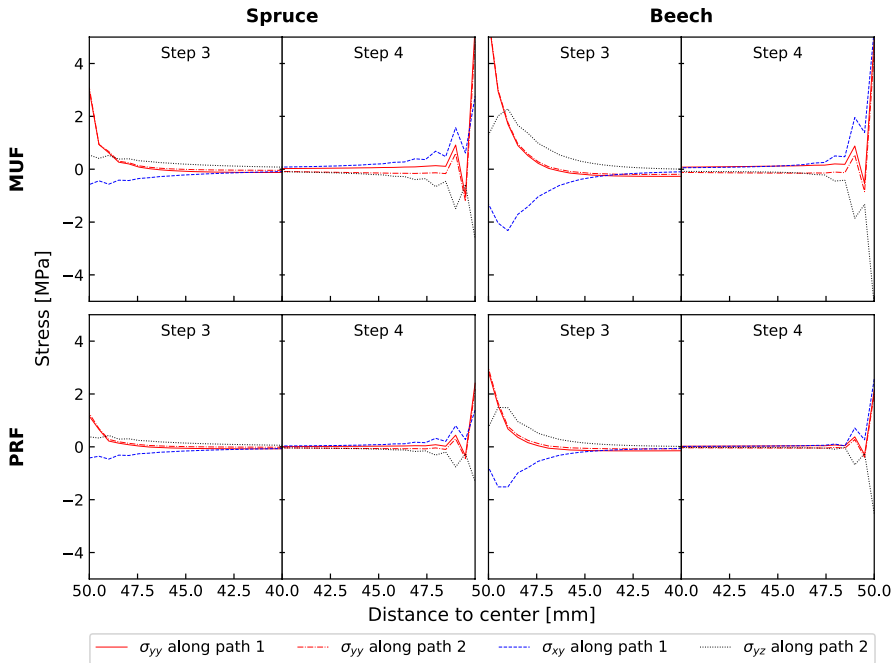


**Fig. 6** Peeling stress  $\sigma_{yy}$  and shear stresses  $\sigma_{xy}$  and  $\sigma_{yz}$  inside the adhesive layer of a CLT plate simulation with  $d = 30$  mm. The curves are taken along the paths 1 and 2, shown in Fig. 3, with the coordinates 0.0 mm being at the center and 50.0 mm being at the respective outer edge of the plate. They document the stresses after removing the sample from the press (step 3) and after re-equilibrating to 65%/20 °C climate (step 4)

**Table 4** Maximum absolute peeling stresses  $\sigma_{yy,i}$  and shear stresses  $\sigma_{xy,i}$  and  $\sigma_{yz,i}$  inside the adhesive layer of the CLT simulation, taken from the paths  $i = 1, 2$ , as shown in Fig. 6

Wood/adhesive	$\sigma_{yy,1}$ [MPa]	$\sigma_{yy,2}$ [MPa]	$\sigma_{xy,1}$ [MPa]	$\sigma_{yz,2}$ [MPa]
<i>Step 3</i>				
Spruce/MUF	2.97	3.09	- 0.58	0.54
Spruce/PRF	1.16	1.26	- 0.46	0.43
Beech/MUF	5.71	5.81	- 2.32	2.28
Beech/PRF	2.85	2.97	- 1.52	1.49
<i>Step 4</i>				
Spruce/MUF	5.39	4.83	2.76	- 2.63
Spruce/PRF	2.41	2.19	1.39	- 1.32
Beech/MUF	4.93	4.44	5.29	- 5.16
Beech/PRF	2.14	2.00	2.57	- 2.53

and water penetration at the moment of hardening in relation to the moisture content at the end of step 3, that is consequently bigger the smaller  $t_{gel}$ .

The observations are consistent to delamination resistance tests conducted for different wood and adhesive types in Konnerth et al. (2016). Here, PRF shows a better performance than MUF and spruce a better performance than beech. This



can partly be explained with the lower amount of residual stresses in the adhesive bondline of the hereby performed FEM simulations.

To quantify the stresses and strains introduced into the whole domain of the CLT system, the total recoverable strain energy  $U$  of the entire model (ALLSE in Abaqus) after step 3 and step 4 is documented in Fig. 7. To know the influence of the wood's layer thickness  $d$  on the total stress/strain potential, a parametric study with increasing  $d$  is evaluated here. The absolute induced moisture, being the only stress-driving parameter during hardening, is for all  $d$  the same, as the properties of the adhesive layer are the same.  $U$  quantifies the work done over the whole plate volume by the introduction of this moisture. For comparability, the thicknesses are chosen in accordance with the CLT plate studies in Hassani et al. (2016).

It can be seen in step 3 (Fig. 7a) that  $U$  is much larger in comparison to step 4 (Fig. 7b). It is assumed that  $U$  in Fig. 7a is strongly influenced by the moisture content that is still present in the CLT sample directly after pressing. Here, a larger  $d$  acts like a constraint that prevents bending and deformation of the plate. Since it induces more moisture into the wood, MUF leads again to larger total strain energies. Once the cross section reaches a certain thickness, the moisture gradient can fully develop without penetrating the whole wood layer. From this thickness onward, the increase of  $U$  over  $d$  is reduced, as it can be seen in Fig. 7a for  $d = 20$  mm to  $d = 30$  mm. Since PRF introduces much less moisture into the system, the full moisture gradient develops for lower  $d$  and a nearly constant and smaller  $U$  is already reached at  $d = 10$  mm. In this system, it can be observed that a higher moisture transport in the wood leads to a higher total strain energy  $U$ .

When evaluating  $U$  after step 4 (Fig. 7b), converse observations can be taken. The most important difference is that with increasing  $d$ , the significantly lower strain energy  $U$  decreases. Since larger  $d$  led to a distribution of the moisture over a larger wood volume, the local water content nearby the adhesive layer during curing was smaller, leading to smaller residual stresses after re-equilibrating. Again, MUF leads to higher residual stresses than PRF. Contrary to step 3, however, the residual stresses are higher for spruce than for beech, respectively. To explain this, the whole moisture input into the wood needs to be interpreted in relation to the dry wood mass. Since spruce has a much lower dry density than beech and the very same mass

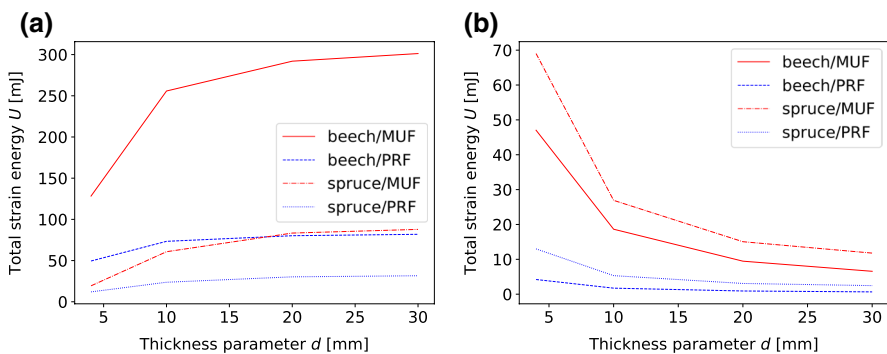


**Fig. 7** Total strain energies of the CLT simulations of all wood/adhesive configurations **a** directly after pressure release (step 3) and **b** at equilibrium climate (step 4) with respect to the thickness parameter  $d$

of moisture gets introduced, spruce's increase in moisture content is larger. The local swelling differences between active and passive layer nearby the adhesive layer were sufficient to result in higher total strain energies  $U$  after re-equilibrating.

With this practical example, the usefulness of the parameters  $t_{\text{gel}}$  and  $\beta$  for estimating residual stresses in larger structures is shown. Whereas moisture change cycles of 20% moisture content for beech CLT plates in Hassani et al. (2016) introduced peeling stresses of 20 MPa (MUF) and 25 MPa (PRF) and shear stresses of 30 MPa (MUF and PRF), these stresses would need to be superposed by 4.9 MPa (MUF) and 2.1 MPa (PRF) residual peeling stresses and 5.3 MPa (MUF) and 2.6 MPa (PRF) residual shear stresses, respectively, at the plate's outer edges. This would be an increase of up to 24.5% stress at its maximum for beech/MUF that would not be respected. In Stapf (2013), shear strengths for MUF, PRF and PUR ranging from 12.7 MPa to 14.1 MPa were determined, indicating that the residual stresses can utilize a significant portion of the total strength. The residual stresses are an upper bound because the model in the present paper is limited to ideal hygro-elasticity without time-dependent influences like relaxation.

## Conclusion

With a combined experimental-numerical approach, it has been possible to quantify the residual stresses introduced by adhesive bonding of wood. This has been made possible by using wood bilayers as reporter systems that show pronounced curvature development during moisture change. Measurement of the curvatures allowed a determination of the parameters describing the wood-adhesive interaction during hardening, making the back-calculation of residual stresses possible in a subsequent step. The residual stresses leading to the observed curvature are the result of the chemical composition and reaction kinetics of cross-linking of the adhesive on the one hand and moisture transport phenomena and dimensional changes of the wood on the other hand. Consistently, the largest stresses could be identified for MUF, which releases the largest amount of water followed by PRF. As PUR rather takes up moisture for cross-linking, inverted behavior was observed, but at much lower level. The calculated stresses in the bilayers are geometry-specific. However, the identified controlling parameters  $t_{\text{gel}}$  and  $\beta$  solely depend on the adhesive system and wood species. Therefore, they can be applied to calculate residual stresses of adhesively bonded timber element systems at any scale. This is a major step forward compared to residual stress calculations in bonded components based on deformation measurements (Scheffler et al. 2007; Hassani et al. 2016; Hänsel et al. 2021). In corresponding simulations of CLT plates, significant residual stresses nearby the outer edges of the plates were identified, with MUF leading to higher residual stresses than PRF and beech having higher moisture gradients during gluing (and therefore higher internal stresses) than spruce. These stresses represent upper limits since effects like plasticity and relaxation are not included in the current model. They will potentially allow to be less conservative than present technical assessment standards.

**Supplementary Information** The online version contains supplementary material available at <https://doi.org/10.1007/s00226-022-01402-0>.

**Acknowledgements** The contribution to this work by Thomas Schnider for sample preparation as well as the financial support from the Swiss National Science Foundation under SNF grant 200021\_192186 "Creep behavior of wood on multiple scales" is acknowledged.

**Author contributions** Conception and methodology: FKW, MR, PG, JMM.; Formal analysis and investigation: All authors. Writing: original draft preparation: JMM, PG, MR, FKW; review and editing: All authors. Supervision: FKW, MR, and PG.

**Funding** Open access funding provided by Swiss Federal Institute of Technology Zurich. Swiss National Science Foundation under SNF grant 200021192186 "Creep behavior of wood on multiple scales".

**Availability of data and materials** Experimental data and simulation data is accessible via <https://doi.org/10.3929/ethz-b-000558245>.

**Code availability** See availability of data and materials.

## Declarations

**Conflict of interest** On behalf of all authors, the corresponding author states that there is no conflict of interest.

**Open Access** This article is licensed under a Creative Commons Attribution 4.0 International License, which permits use, sharing, adaptation, distribution and reproduction in any medium or format, as long as you give appropriate credit to the original author(s) and the source, provide a link to the Creative Commons licence, and indicate if changes were made. The images or other third party material in this article are included in the article's Creative Commons licence, unless indicated otherwise in a credit line to the material. If material is not included in the article's Creative Commons licence and your intended use is not permitted by statutory regulation or exceeds the permitted use, you will need to obtain permission directly from the copyright holder. To view a copy of this licence, visit <http://creativecommons.org/licenses/by/4.0/>.

## References

- Archer RR (1987) Growth stresses and strains in trees. Springer series in wood science, 1st edn. Springer, Berlin
- ASTM D4501 (2014) Standard test method for shear strength of adhesive bonds between rigid substrates by the block-shear method. Standard ASTM D4501-01, ASTM International
- Bachtiar EV, Konopka D, Schmidt B, Niemz P, Kaliske M (2019) Hygro-mechanical analysis of wood-adhesive joints. Eng Struct 193:258–270
- BASF (2007) KAURAMIN Leim 683 flüssig mit KAURAMIN Härter 688 flüssig im Holzleimbau [KAURAMIN glue 683 liquid with KAURAMIN hardener 688 liquid for adhesively bonded wood construction]. Technical Report M 6220 d, BASF Aktiengesellschaft
- Bolleter Composites (2009) Aerodux 185 RL / Härter HP 155 [Aerodux 185 RL / Hardener HP 155]. Technical Report, Bolleter Composites AG
- DIN EN 301 (2017) Adhesives, phenolic and aminoplastic, for load-bearing timber structures – classification and performance requirements. Standard EN 301:2017, DIN Deutsches Institut für Normung e. V
- DIN EN 302-1 (2013) Adhesives for load-bearing timber structures – test methods – part 1: determination of longitudinal tensile shear strength. Standard EN 302-1:2013, DIN Deutsches Institut für Normung e. V
- DIN EN 302-2 (2017) Adhesives for load-bearing timber structures – test methods – part 2: determination of resistance to delamination. Standard EN 302-2:2017, DIN Deutsches Institut für Normung e. V

- Gereke T (2009) Moisture-induced stresses in cross-laminated wood panels. Ph.D. thesis, ETH Zurich
- Gindl W, Schöberl T, Jeronimidis G (2004) The interphase in phenol-formaldehyde and polymeric methylene di-phenyl-di-isocyanate glue lines in wood. *Int J Adhes Adhes* 24(4):279–286
- Grönquist P, Wittel FK, Rüggeberg M (2018) Modeling and design of thin bending wooden bilayers. *PLoS ONE* 13(10):e0205607
- Grönquist P, Wood D, Hassani MM, Wittel FK, Menges A, Rüggeberg M (2019) Analysis of hygroscopic self-shaping wood at large-scale for curved mass timber structures application. *Sci Adv* 5:eaax1311
- Hass P, Wittel FK, Mendoza M, Herrmann HJ, Niemz P (2012) Adhesive penetration in beech wood: experiments. *Wood Sci Technol* 46(1–3):243–256
- Hassani MM, Wittel FK, Ammann S, Niemz P, Herrmann HJ (2016) Moisture-induced damage evolution in laminated beech. *Wood Sci Technol* 50(5):917–940
- Hassani MM, Wittel FK, Hering S, Herrmann HJ (2015) Rheological model for wood. *Comput Methods Appl Mech Eng* 283:1032–1060
- Hunt CG, Frihart CR, Dunky M, Rohumaa A (2019) Understanding wood bonds-going beyond what meets the eye: a critical review. In: *Progress in adhesion and adhesives*. Wiley
- Hänsel A, Sandak J, Sandak A, Mai J, Niemz P (2021) Selected previous findings on the factors influencing the gluing quality of solid wood products in timber construction and possible developments: a review. *Wood Mater Sci Eng* 17(3):230–241
- Knorz M, Niemz P, van de Kuilen J-W (2016) Measurement of moisture-related strain in bonded ash depending on adhesive type and glue line thickness. *Holzforschung* 70(2):145–155
- Knorz M, Torno S, van de Kuilen J-W (2017) Bonding quality of industrially produced cross-laminated timber (CLT) as determined in delamination tests. *Constr Build Mater* 133:219–225
- Kollmann FF, Cote WA (1968) *Principles of wood science and technology I solid wood*, 1st edn. Springer, Berlin
- Kollmann FF, Kuenzi E, Stamm A (1975) *Principles of wood science and technology II wood based materials*, 1st edn. Springer, Berlin
- Konnerth J, Harper D, Lee S-H, Rials TG, Gindl W (2008) Adhesive penetration of wood cell walls investigated by scanning thermal microscopy (SThM). *Holzforschung* 62(1):91–98
- Konnerth J, Kluge M, Schweizer G, Miljković M, Gindl-Altmatter W (2016) Survey of selected adhesive bonding properties of nine European softwood and hardwood species. *Eur J Wood Prod* 74(6):809–819
- Kumar RN, Pizzi A (2019) *Adhesives for wood and lignocellulosic materials*. Wiley, Hoboken
- Li L, Gong M, Chui YH, Liu Y (2016) Modeling of the cupping of two-layer laminated densified wood products subjected to moisture and temperature fluctuations: model development. *Wood Sci Technol* 50(1):23–37
- Mendoza M, Hass P, Wittel FK, Niemz P, Herrmann HJ (2012) Adhesive penetration of hardwood: a generic penetration model. *Wood Sci Technol* 46:529–549
- Mueller J (2014) MATSuMoTo: the MATLAB surrogate model toolbox for computationally expensive black-box global optimization problems. arXiv e-prints, P. [arXiv:1404.4261](https://arxiv.org/abs/1404.4261)
- Niemz P, Sonderegger W (2017) *Holzphysik: Physik des Holzes und der Holzwerkstoffe* [Wood physics: physics of wood and wood materials]. Carl Hanser Verlag GmbH & Co. KG, Munich
- Okkonen EA, River BH (1989) Factors affecting the strength of block-shear specimens. *For Prod J* 39(1):43–50
- Purbond (2011) 1K-Polyurethanklebstoff zur Herstellung von tragenden Holzbauteilen [1K-Polyurethane for the creation of load-bearing wooden construction parts]. Technical Report HB S309, Purbond AG
- Rindler A, Vay O, Hansmann C, Konnerth J (2019) Adhesive-related warping of thin wooden bilayers. *Wood Sci Technol* 53:1015–1033
- Rüggeberg M, Burgert I (2015) Bio-inspired wooden actuators for large scale applications. *PLoS ONE* 10(4):e0120718
- Scheffler M, Weber T, Niemz P, Hardtke H-J (2007) Determination of residual stress in bonded wood components. *Holzforschung* 61:285–290
- Siau JF (1984) Transport processes in wood, number 2 in Springer series in wood science. Springer, Berlin
- Skaar C (1988) *Wood–water relations*, Springer series in wood science. Springer, Berlin
- Stapf G, Zisi N, Aicher S (2013) Curing behaviour of structural wood adhesives-parallel plate rheometer results. *Pro Ligno* 9:109–117

- Timoshenko S (1925) Analysis of bi-metal thermostats. *J Opt Soc Am Rev Sci Instrum* 11(3):233–255
- Wimmer R, Kläusler O, Niemz P (2013) Water sorption mechanisms of commercial wood adhesive films. *Wood Sci Technol* 47:763–775
- Wood D, Vailati C, Menges A, Rüggeberg M (2018) Hygroscopically actuated wood elements for weather responsive and self-forming building parts – facilitating upscaling and complex shape changes. *Constr Build Mater* 165:782–791
- Zhu E, Zhou H (2010) Simulation of residual stress in curved glulam beams during manufacturing. In: 11th World Conference on Timber Engineering 2010, vol 1, pp 780–785

**Publisher's Note** Springer Nature remains neutral with regard to jurisdictional claims in published maps and institutional affiliations.

## Authors and Affiliations

Jonas Matthias Maas<sup>1</sup>  · Phillipe Grönquist<sup>2</sup>  · Jennifer Furrer<sup>1</sup>  ·  
Vanessa Studer<sup>1</sup> · Anselmo Malveti<sup>1</sup>  · Markus Rüggeberg<sup>1,3</sup>  ·  
Falk K. Wittel<sup>1</sup> 

Phillipe Grönquist  
groenquist@ibk.baug.ethz.ch

Jennifer Furrer  
jennifer.furrer@alumni.ethz.ch

Vanessa Studer  
V.Studer@htb-ag.ch

Anselmo Malveti  
manselmo@student.ethz.ch

Markus Rüggeberg  
markus.rueggeberg@tu-dresden.de

Falk K. Wittel  
fwittel@ethz.ch

<sup>1</sup> Institute for Building Materials, ETH Zurich, Leopold-Ruzicka-Weg 4, 8093 Zurich, Switzerland

<sup>2</sup> Institute of Structural Engineering – Timber Structures, ETH Zurich, Stefano-Franscini-Platz 5, 8093 Zurich, Switzerland

<sup>3</sup> Present Address: Institute of Forest Utilization and Forest Technology, TU Dresden, Piener Straße 19, 01037 Tharandt, Germany